Supplemental Materials

Anisotropic Electroactive Elastomer for Highly Maneuverable Soft Robotics

Youhua Xiao[1,4,#], Jie Mao[1,#], Yejie Shan[4], Tao Yang[4], Zheqi Chen[1], Fanghao Zhou[4], Jin He[1], Junjie Zhao[1,2], Tiefeng Li[3,4*], Yingwu Luo,[1,2,4*]*

1. The State Key Laboratory of Chemical Engineering, College of Chemical and Biological Engineering, Zhejiang University, 310027, China.
2. Institute of Zhejiang University – Quzhou, Quzhou 324000, China
3. Center for X-mechanics, Zhejiang University, Hangzhou, 310027, China
4. Key Laboratory of Soft Machines and Smart Devices of Zhejiang Province, Department of Engineering Mechanics, Zhejiang University, Hangzhou, 310027, China.

[#] These authors contributed equally to this work.

Corresponding email address: junjiezhao@zju.edu.cn, litiefeng@zju.edu.cn, yingwu.luo@zju.edu.cn

Materials and Methods

Characterization: The molecular weight and molecular weight distribution were measured by Gel Permeation Chromatography (waters 1525/2414) with polystyrene as a calibration standard. The thickness of SBAS thin films were measured by Filmetrics F20-NIR. Tensile measurements were performed on a testing machine (UTM2102) equipped with a 50 N load cell. The species (the gauge length and width were 15 mm 2 mm, respectively) were cut into a dog bone-shape using laser cutting machine. The loading rate was 30 mm/min. The dynamic mechanical properties of the samples (20 mm × 5 mm × 1 mm) were carried out using DMA Q800 instrument with frequency of 5 Hz. The temperature was increased from -90 ℃ to 150 ℃ with a rate of 10 ℃/min. Atomic Force Microscope images were obtained on a Scanning Probe Microscope (Veeco, Multimode) in the tapping mode. Transmission Electron Microscope images were obtained on a JEOL JEMACRO-1230. The samples were stained by RuO_4. The block force of a bending actuator was tested by the electronic balance (FA1004). The dielectric permittivity was measured using a broadband dielectric spectrometer (Novocontrol) from 0.1 Hz to 10^6 at 25 ℃.

The fabrication of a SBAS thin film via solution casting: The triblock copolymer SBAS with design molecular weights for each block being 15, 120 and 15 kDa was synthesized via reversible addition-fragmentation transfer (RAFT) emulsion polymerization according to our previous work (*1*). SBAS copolymers were dissolved into tetrahydrofuran to form a 10 wt% solution. Then, the polymer solution was casted on an anti-sticking PET substrate with 1000 μm thickness. The blading speed was 2 mm/min. The room-temperature-dried film was annealed at 120 ℃ for 8 h under vacuum. Finally, the pristine SBAS film was achieved with thickness of around

75 μm. All the processes were carried out in an argon atmosphere.

The PSTR treatment of SBAS films: SBAS films (75 μm) were uniaxially pre-stretched to 2, 4, and 6 times of their initial length, respectively. The pre-stretched film was self-adhered on an anti-sticking PET substrate. Then, The pre-stretched films were relaxed at 120 ℃ for 8 h. After the thermal relaxation, the SBAS films were peeled off the PET substrate at room temperature to release the residual stress for at least 2 hours to collect the anisotropic SBAS films.

The fabrication of a circular DE actuator: A circular actuator was fabricated by fixing a PSTR treated SBAS thin film on a circular rigid frame without additional pre-stretching. The diameter of the circular actuator was 60 mm. The SWCNT electrodes (the sheet resistance was about 2-3 kΩ/sq) (*2*) were transferred on the center of both sides of SBAS film in a circular shape with 15 mm diameter.

The fabrication of stacked actuators in isotonic (constant force) configuration: DE stacked rectangular actuators (6 mm × 50 mm), consisting of ten active SBAS layers (thickness: 22 μm per layer) were fabricated into isotonic configuration. The active DE layers were sandwiched between two SWCNT electrodes. The electrode area was 5 mm × 30 mm with the blank margin of 0.5 mm. Two ends along the actuator length were clamped by PET sheets.

The fabrication of stacked bending actuators: The DE rectangular bending actuator (6 mm × 21 mm), consisted of ten active SBAS layers (thickness: 22 μm per layer), one adhesive layer (SBAS, 22 μm) and one passive PET layer (10 μm, Young's modulus: 2 GPa). The active DE layers were sandwiched between two SWCNT electrodes (the sheet resistance was about 2-3 kΩ/sq). The electrode area was 5 mm × 20 mm with the blank margin of 0.5 mm. One end of the bending actuator was clamped by PET sheets.

The fabrication of a crawling soft robot: The DE bending actuator (6 mm × 25 mm), consists 30 active SBAS layers (thickness: 22 μm per layer), one adhesive layer (SBAS, 22 μm) and one passive PET layer (10 μm, Young's modulus: 2 GPa). The active DE layers were sandwiched between two SWCNT electrodes (the sheet resistance is about 2-3 kΩ/sq). The electrode area is 5 mm × 20 mm and the size of the three margins is 0.5 mm, the rest margin is 5 mm. Then, two bending actuators were symmetrically assembled together using hot melt adhesive to fabricate a directional soft robot. The body length of soft robot is about 5.7 mm, and the whole weight of the soft robot is about 0.45g.

Finite element simulation using ABAQUS: To model the wrinkling behavior of the circular DE actuator of the anisotropic SBAS film, a two-step approach was presented. In the first step, a cubic model represented a small part of the active zone of the actuator was established. Without the constraints from the surrounding passive zone, this cubic model could help to calculate the free deformations of the active zone along three material directions under Maxwell pressure. In the second step, the deformations obtained in the first step were applied to the active zone directly. Due to the constraints from the surrounding passive zone, the active zone exhibited the wrinkling behavior. *First step:* Considering the small strain during wrinkling process, linear elasticity instead of hyper-elasticity was adopted as the constitutive model. We considered the film as a transversely isotropic plate. The material constants were listed in Table S2. Then, the deformations induced by the voltages were readily obtained by applying a pressure directly onto the top and bottom surfaces. The Maxwell pressure was calculated as: $\sigma_{max} = \varepsilon_0 \varepsilon_r E^2 = \varepsilon_0 \varepsilon_r (U/d)^2$. In which, ε_0=8.85 × 10^{-12} F/m is the dielectric constant in vacuum, ε_r is the relative dielectric constant, E is the electric field, U is the driving voltage, and d is the thickness of DE film. In this step, a 1/8 model was established and 50 8-node linear brick elements with reduced integration (C3D8R) were meshed. *Second step:* In the second step, the model was established according to the geometric sizes of the actuators. The deformations were applied to the active zone as follows: assume the film should have three thermal expansion coefficients along three material directions; make each thermal expansion coefficient be equal to the corresponding deformation obtained in the first step, respectively; apply a temperature load which is 1 ℃ to the active area. Besides, to generate wrinkling phenomenon, a perturbation or imperfection should be included in the model. This imperfection should be large enough to make the model buckle locally while small enough to maintain the precision of the solution. In our model, a slight body force as the perturbation was applied to play this role. The model was meshed with 32800 4-node doubly curved shell elements with reduced integration (S4R).

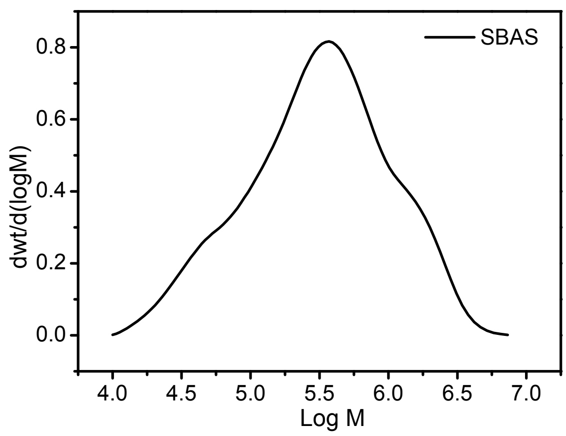

Fig. S1 GPC curve of the triblock copolymer SBAS

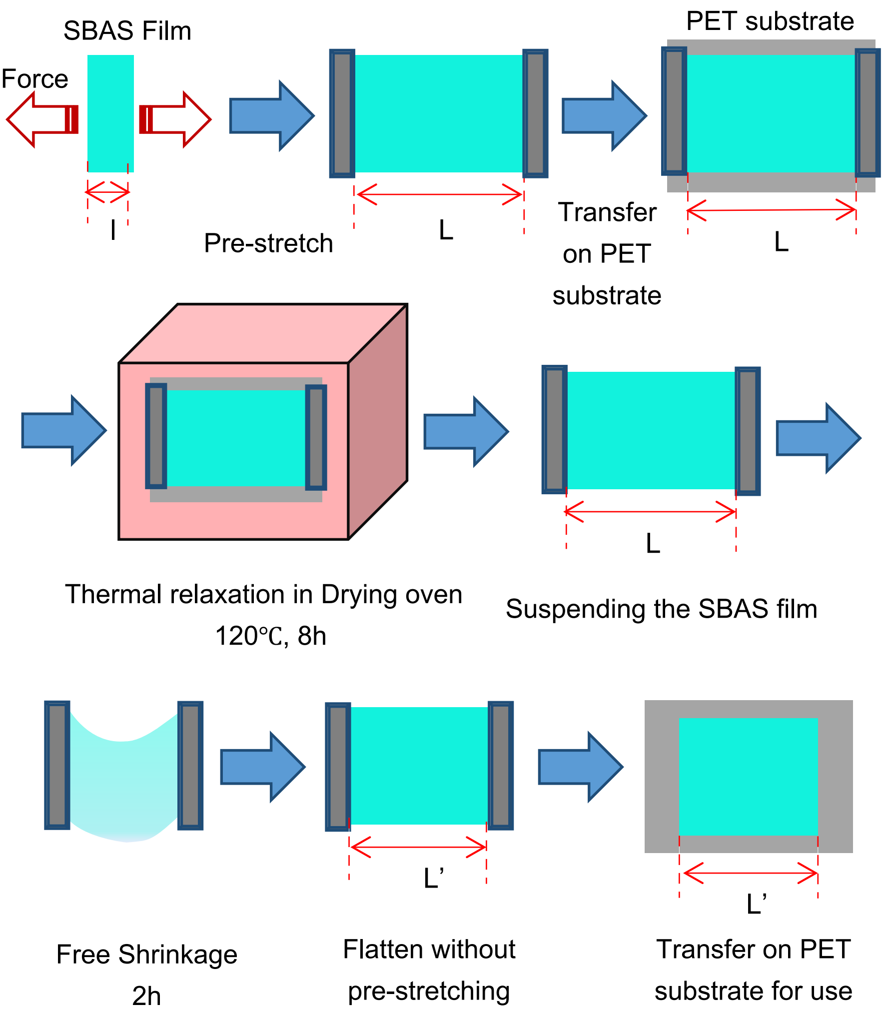

Fig. S2 Sequence of operations to produce a uniaxial PSTR treated SBAS film.

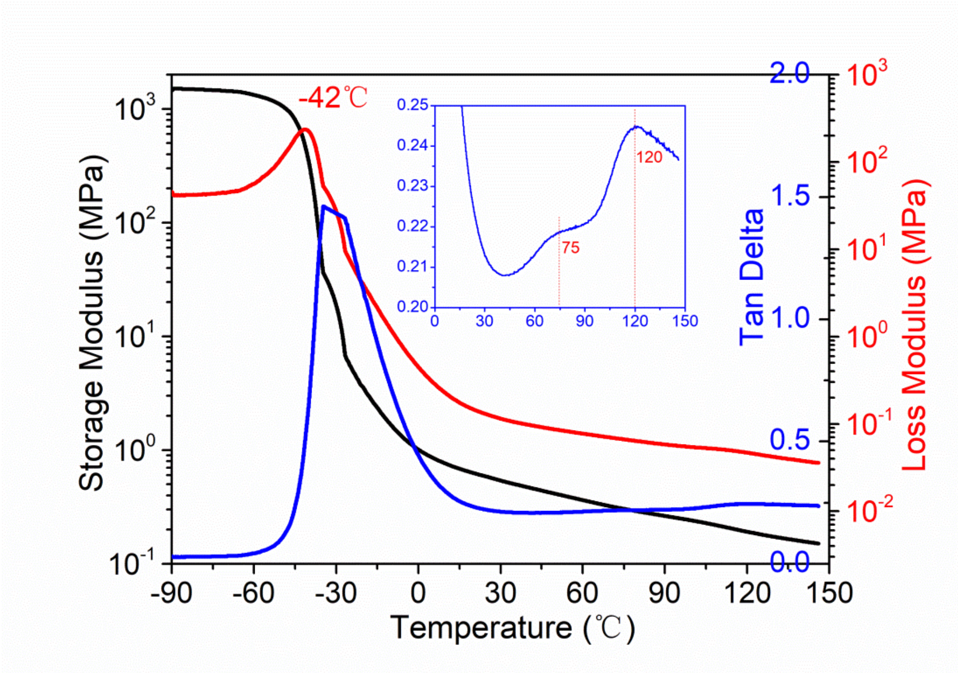

Fig. S3 DMA characterization of SBAS film. The inserted graph is the zoomed in graph of Tan Delta plot, which shows the glass transition temperature of PS block is below 120 ℃.

Table S1. The elongation of SBAS films during uniaxial PSTR treatment

	Designed elongation (%)	Shrinkage (%)	Left prestrech (%)	Standard deviation of shrinkage
L/l=2	100	9.21	90.79	1.41
L/l=4	300	22.49	232.53	4.69
L/l=6	500	16.35	418.25	1.12

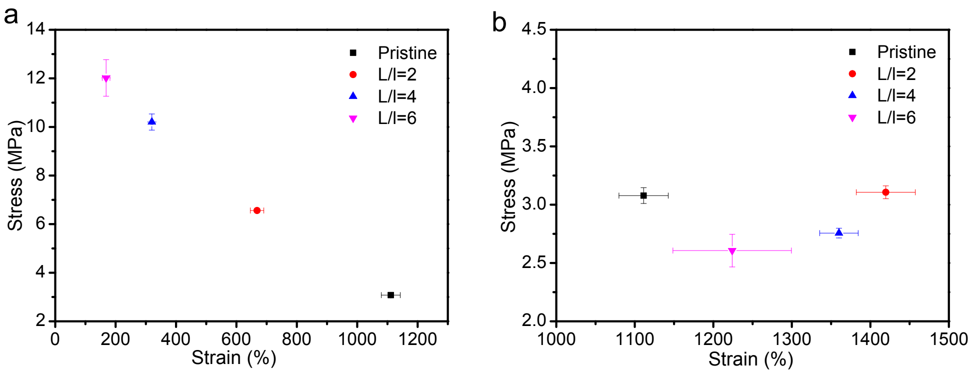

Fig. S4 (**a**) The error bars are standard deviations of break strength versus ultimate elongation along the parallel direction of uniaxial PSTR treatment. (**b)** The error bars are standard deviations of break strength versus ultimate elongation along the perpendicular direction of uniaxial PSTR treatment.

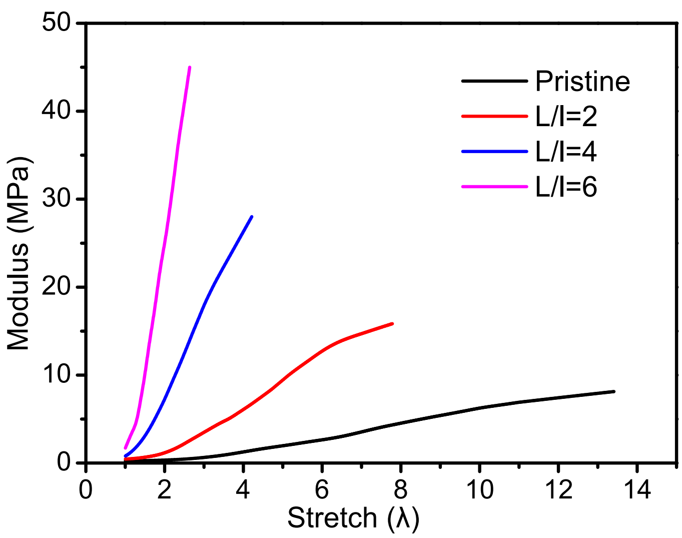

Fig. S5 Modulus versus stretch curves of SBAS with different uniaxial prestrech ratio along the parallel direction of PSTR treatment.

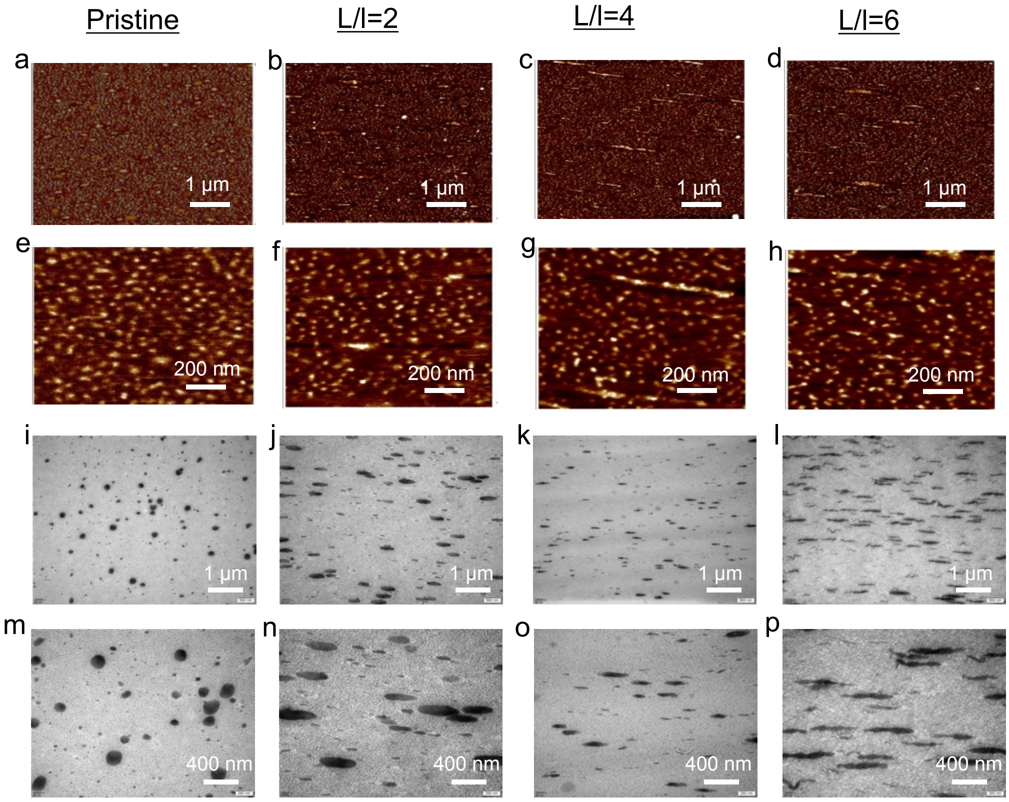

Fig. S6 AFM and TEM images of SBAS films under uniaxial PSTR treatment with different stretch ratios. (**a,e,i,m**), (**b,f,j,n**), (**c,g,k,o**) and (**d,h,l,p**) are corresponding to the original SBAS films, 2 times, 4 times and 6 times prestretched treatment, respectively.

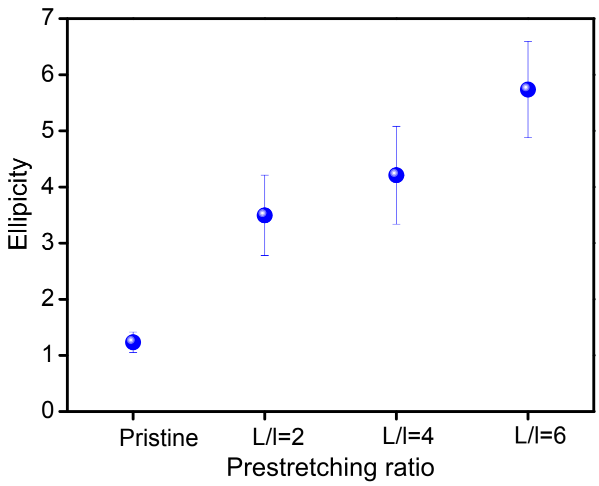

Fig. S7, The ellipticity of PS domains in SBAS versus prestretching ratio (Statistic data from over 60 domains presented in Fig.S9).

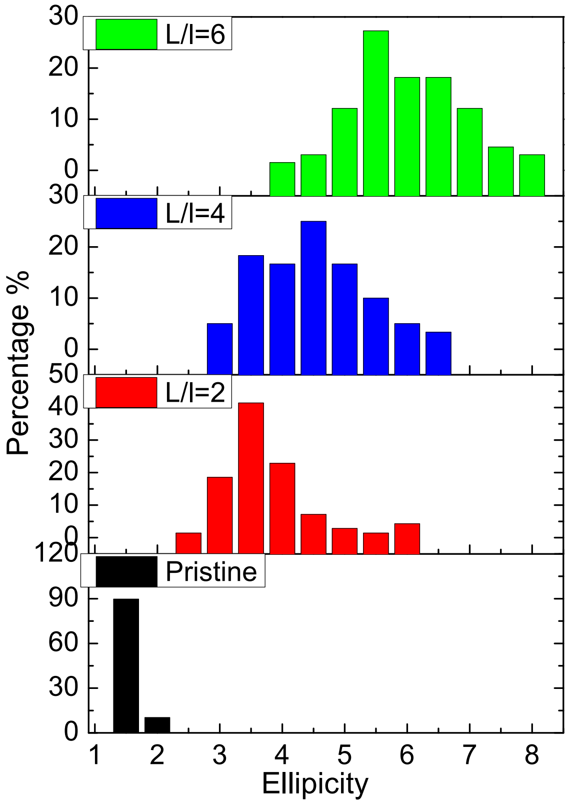

Fig. S8 The histograms of ellipticity according to Fig. S9.

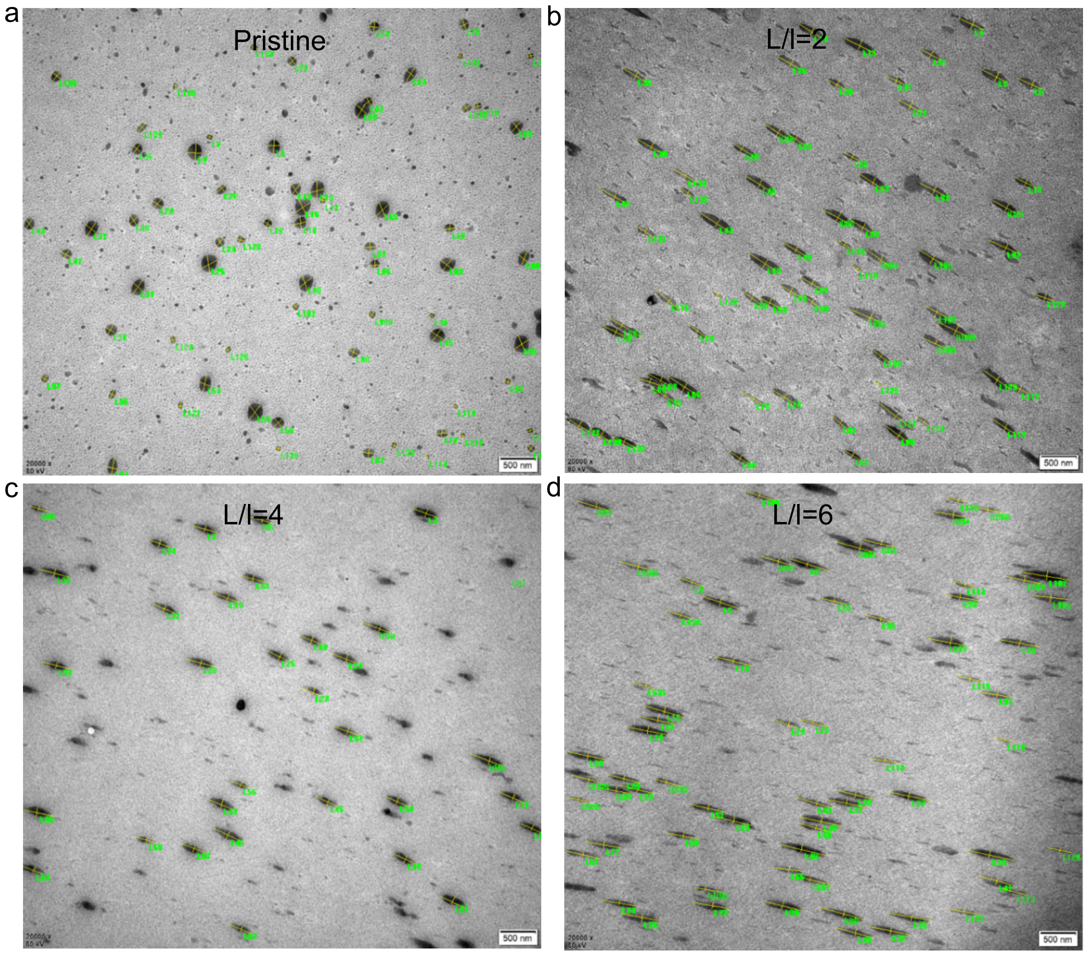

Fig. S9 (**a,b,c,d**)The TEM images of PSTR treated SBAS samples with different prestetching ratios were used for calculating the ellipticity. The green lines were the drawing trace used for calculating the ellipticity of PS domains.

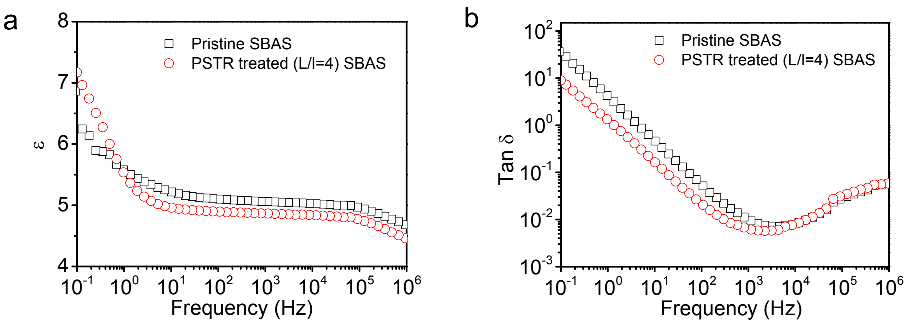

Fig. S10 Dielectric properties of PSTR treated SBAS: (a) Dielectric relative permittivity; (b) Dielectric loss.

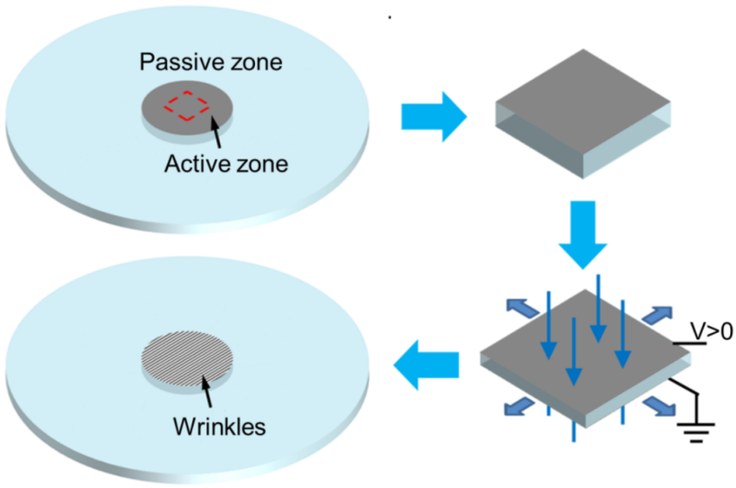

Fig. S11 The schematic diagram of the two-step approach for mechanical simulation of circular actuators.

Table S2. The material constants, thicknesses and applied voltages of the actuators.

Enter	E_1 (MPa)	E_2 (MPa)	G_{12} (MPa)	v_{21}	v_{23}	ε_r	t(mm)	U(V)
Pristine	0.3		0.10	0.499			0.075	2400
L/l=2	0.7		0.35				0.055	1400
L/l=4	3.5	0.3	1.73	0.01	0.499	4.8	0.022	800
L/l=6	10.5		5.20				0.012	650

Note: The subscript number 1, 2 mean the direction parallel or perpendicular direction to the prestretch direction, respectively. The subscript number 3 means the direction of thickness. E_1, E_2 are the Young's modulus (at 50% strain according to Fig. S5) of the uniaxial PSTR treated SBAS films along the parallel or perpendicular direction, respectively. G_{12}, is the shear modulus in the face of 1,2 plane. v_{12} characterize the transverse strain in the 2 direction, when the material is stressed in the 1 direction. v_{23} characterize the transverse strain in the 3 direction, when the material is stressed in the 2 direction. ε_r, The relative permittivity of dielectric elastomers. t, The thickness of SBAS films. U, The driving voltages. Here, we assumed that v_{21}=0.01 due to $E_1>E_2$. And there are two equations can be used to illustrate the relationship between each constant: $\frac{E_1}{v_{12}}=\frac{E_2}{v_{21}}$, $G_{12}=\frac{E_1}{2*(1+v_{21})}$.

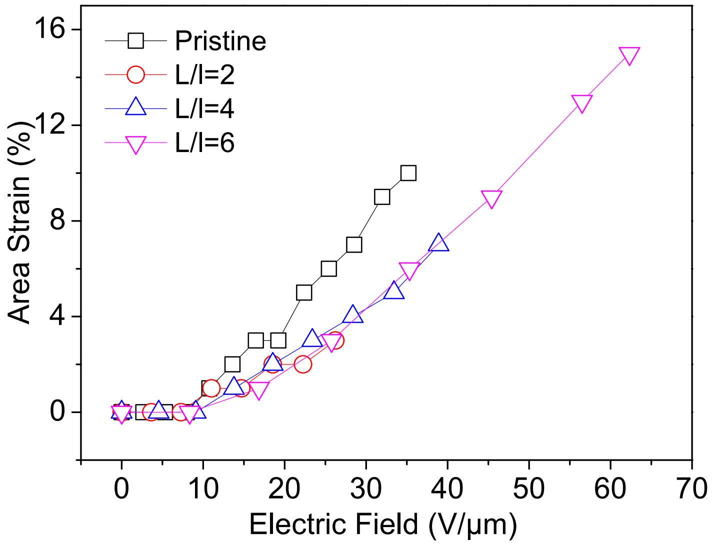

Fig. S12 The electric field versus area strain curves according to the mechanical simulation by using the experimental data.

Fig. S13 (**a,b**) The photos of DE actuator in the state of driving on/off, respectively. The actuator was fabricated into isotonic configuration with **D** ⊥ **S** by using anisotropic SBAS film.

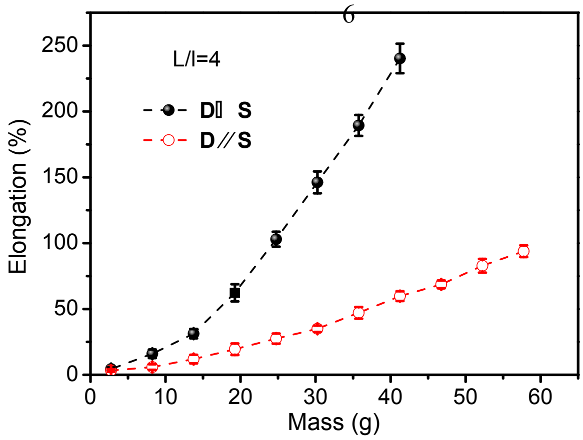

Fig. S14 The elongation of actuators versus loading mass for strain directions parallel (**D**//**S**) or perpendicular (**D**⊥**S**) to the PS domain orientation (pre-stretch ratio L/l=4).

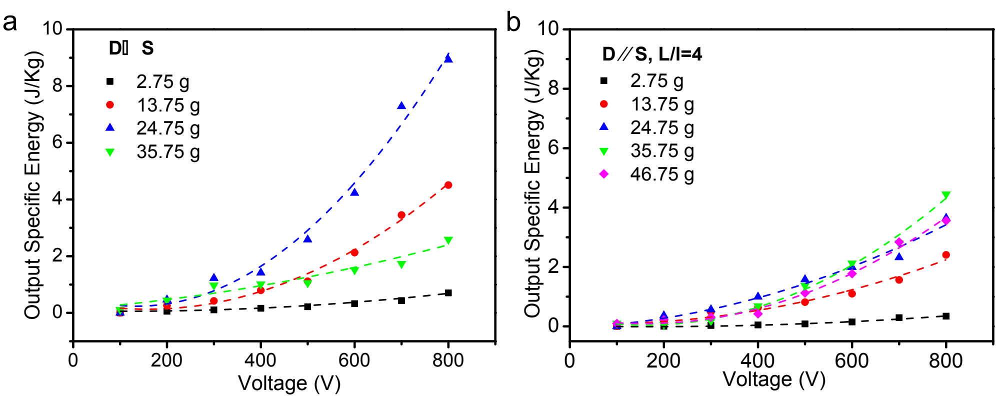

Fig. S15 (**a,b**) The output specific energy versus driving voltage under different loading mass of the anisotropic actuators with **D**⊥**S** and **D**//**S** configuration, respectively.

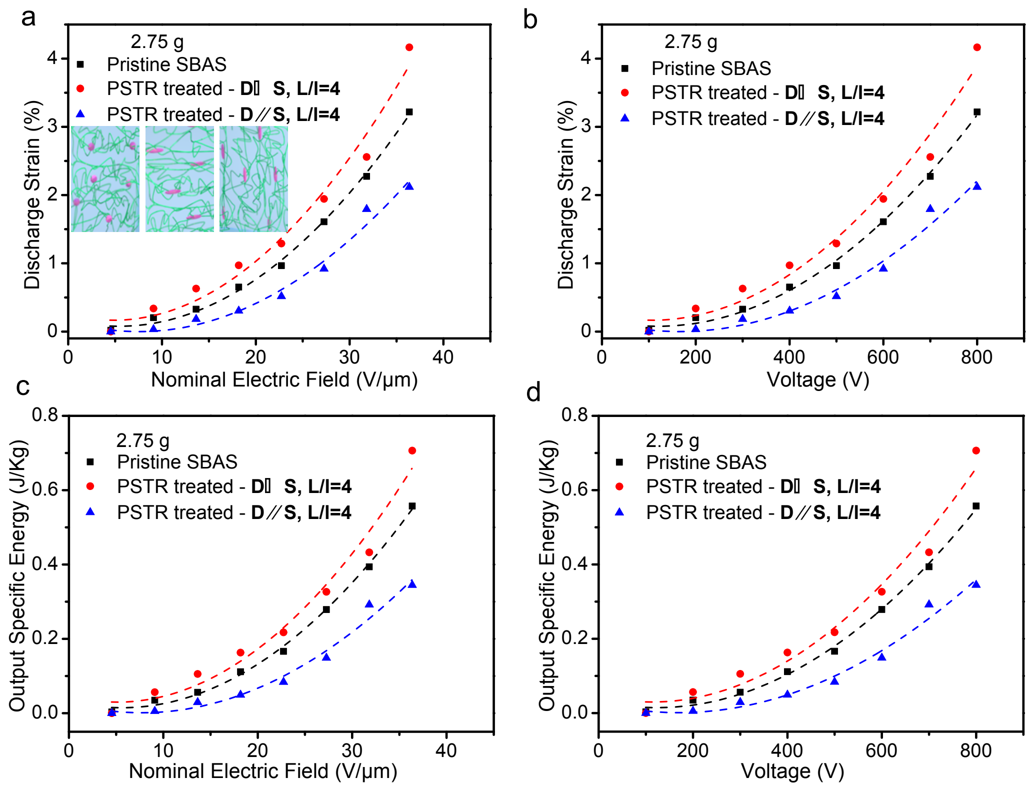

Fig. S16 (**a**) The comparison of discharge strain versus driving voltage between actuators in isotonic configuration (loaded with 2.75g) by using pristine SBAS film or uniaxial PSTR treated SBAS films (**D**⊥**S** and **D**//**S**). (**b**) The comparison of output specific energy versus driving voltage between actuators in isotonic configuration (loaded with 2.75g) by using pristine SBAS film or uniaxial PSTR treated SBAS films (**D**⊥**S** and **D**//**S**).

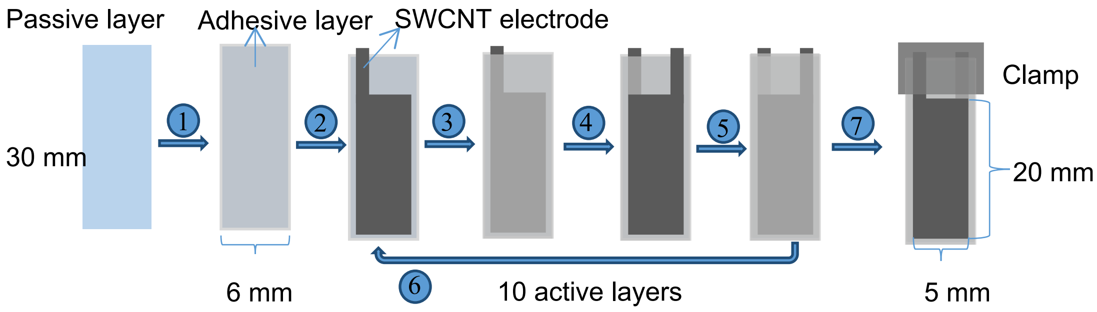

Fig. S17 The schematic illustration of preparing stacked bending actuator.

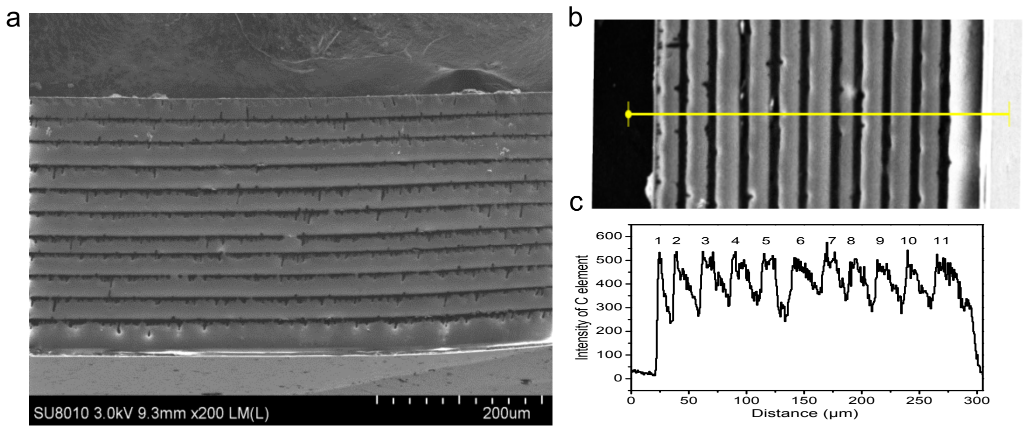

Fig. S18 (**a**, **b**) SEM images of the cross section of the stacked bending actuator. (**c**) The curve of carbon intensity versus distance along the yellow line in (**b**).

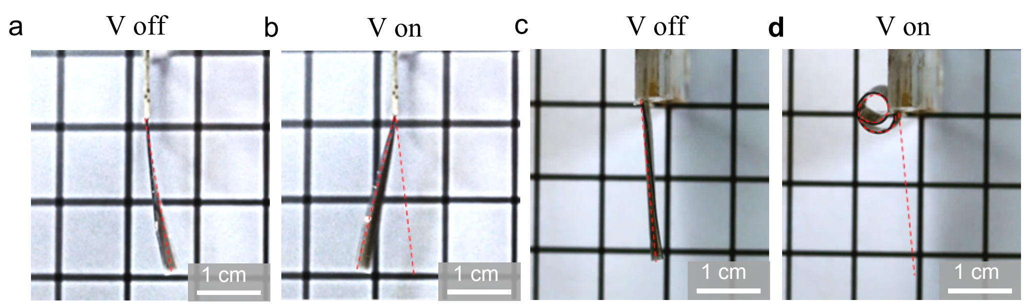

Fig. S19 (**a**,**b**) The static state and actuated state of the bending actuator using pristine SBAS films. (**c**,**d**) the static state and actuated state of the bending actuator using anisotropic SBAS films (at 800V).

Mechanical analysis of bending actuator:

The bending degree of the bending actuator is determined by the flexural rigidity under the same bending moment. The flexural rigidity is determined by the cross sectional moment of inertia when using the same material with same elastic modulus. Hence, the higher cross sectional moment of inertia leads to higher flexural rigidity, which indicates harder to be bent.

$$\frac{1}{\rho}=\frac{M}{EI} \quad \cdots\cdots\cdots\cdots\cdots\cdots\cdots\cdots \quad (1)$$

ρ: Radius of curvature, M: Bending moment, E: Elastic modulus, EI: Flexural rigidity, I: Cross sectional moment of inertia

From the result of Fig. S16, the bending actuator made of PSTR treated SBAS films (L/l=4) can be bent into a circle shape due to the higher modulus in the width direction (Fig. S17a). In contrast, the bending actuator using pristine SBAS films can simultaneously bend in its width direction, which would decrease the radius of curvature (Fig. S17b). Here, we qualitatively analyzed the relationship between the cross sectional moment of inertia and the radius of curvature under electric activated deformation of the bending actuators (Fig. S17c).

First, we assumed y_0 is the neutral layer of the cross section of bending actuator. The cross sectional moment of inertia can be calculated from equation (2) according to the mechanics of materials.

$$\mathrm{I}=\int (y-y_0)^2 dA=\int \left(y^2-2y_0y+y_0{}^2\right)dA=\int y^2dA-2y_0\int ydA+y_0{}^2\int dA \quad \cdots\cdots\cdots \quad (2)$$

The resultant force of couple at the neutral layer is zero, so:

$$\int E\,(y-y_0)\,dA=0$$

$$\therefore \int ydA=\int y_0dA$$

$$\therefore y_0=\frac{\int ydA}{bh}$$

The area of cross section of bending actuator was calculated as:

$$dA=\int \frac{(r+dr)^2-r^2}{2}d\theta \approx rdrd\theta \quad \cdots\cdots\cdots\cdots\cdots\cdots \quad (4)$$

$$\therefore \int ydA=\int_{\rho'-\frac{h}{2}}^{\rho'+\frac{h}{2}}\int_{\frac{\pi}{2}-\frac{b}{2\rho'}}^{\frac{\pi}{2}+\frac{b}{2\rho'}} rsin\theta rdrd\theta=\frac{2}{3}\left[\left(\rho'+\frac{h}{2}\right)^3-\left(\rho'-\frac{h}{2}\right)^3\right]\sin\frac{b}{2\rho'}$$

$$\therefore y_0=\frac{\int ydA}{bh}=\frac{2}{3bh}\left[\left(\rho'+\frac{h}{2}\right)^3-\left(\rho'-\frac{h}{2}\right)^3\right]sin\frac{b}{2\rho'} \quad \cdots\cdots\cdots\cdots\cdots \quad (5)$$

$$\therefore y_0^2\int dA = y_0^2 bh \cdots\cdots\cdots\cdots\cdots\cdots \quad (6)$$

$$\therefore 2y_0\int ydA = \frac{4y_0}{3}\left[\left(\rho' + \frac{h}{2}\right)^3 - \left(\rho' - \frac{h}{2}\right)^3\right] sin\frac{b}{2\rho'} \cdots\cdots\cdots \quad (7)$$

$$\therefore \int y^2 dA = \int_{\rho'-\frac{h}{2}}^{\rho'+\frac{h}{2}}\int_{\frac{\pi}{2}-\frac{b}{2\rho'}}^{\frac{\pi}{2}+\frac{b}{2\rho'}} (rsin\theta)2rdrd\theta = (\frac{b}{2\rho'} + \frac{1}{2}\sin\frac{b}{\rho'})\left(\frac{\left(\rho' + \frac{h}{2}\right)^4 - \left(\rho' - \frac{h}{2}\right)^4}{4}\right)$$

$$\cdots\cdots\cdots\cdots\cdots\cdots \quad (8)$$

Combined equation (6-8) into equation (2), the cross sectional moment of inertia is:

$$\mathrm{I} = \int y^2 dA - 2y_0\int ydA + y_0^2\int dA$$

$$= (\frac{b}{2\rho'} + \frac{1}{2}\sin\frac{b}{\rho'})\left(\frac{\left(\rho' + \frac{h}{2}\right)^4 - \left(\rho' - \frac{h}{2}\right)^4}{4}\right) - \frac{4}{9bh}\left\{\left[\left(\rho' + \frac{h}{2}\right)^3 - \left(\rho' - \frac{h}{2}\right)^3\right]\sin\frac{b}{2\rho'}\right\}^2$$

When $\rho' \to +\infty$, then $\mathrm{I_{in}} = \frac{\mathrm{bh}^3}{12}$, which is the cross sectional moment of inertia of initial rectangle. Here, we assumed the b=6 mm, h=250 μm, then used the Matlab to draw the plot of $\mathrm{I/I_{in}}$ versus ρ' (Fig. S18).

Qualitatively, the $\mathrm{I/I_{in}}$ increases sharply following the decrease of radius of curvature ρ', which would induce the increase of flexural rigidity. So, the bending actuator using pristine SBAS films can simultaneously bend in its width direction, which would decrease the radius of curvature and increase the cross sectional moment of inertia. This would increase the flexural rigidity of the bending actuator.

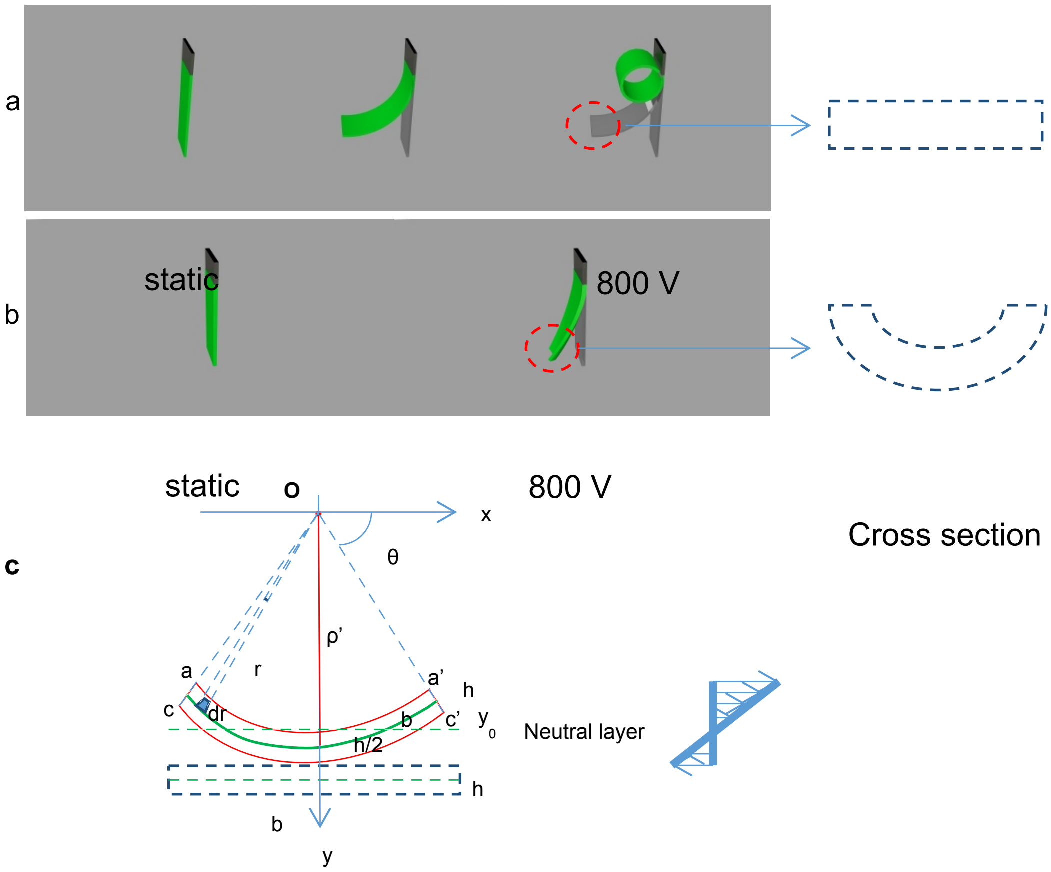

Fig. S20 (**a, b**) The cross section of the two kind bending actuators made of uniaxial PSTR treated SBAS films (L/l=4) (**a**) and pristine SBAS films (**b**) were compared. The cross section of bending actuator using pristine SBAS films has higher curvature. **c** The coordinate of the cross section of actuated bending actuator was established to make a mechanical analysis (at 800V).

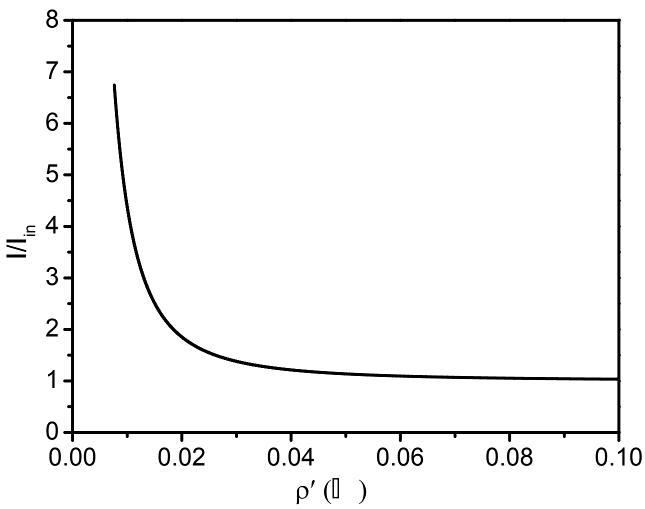

Fig. S21 The relationship between I/I_{in} and ρ'.

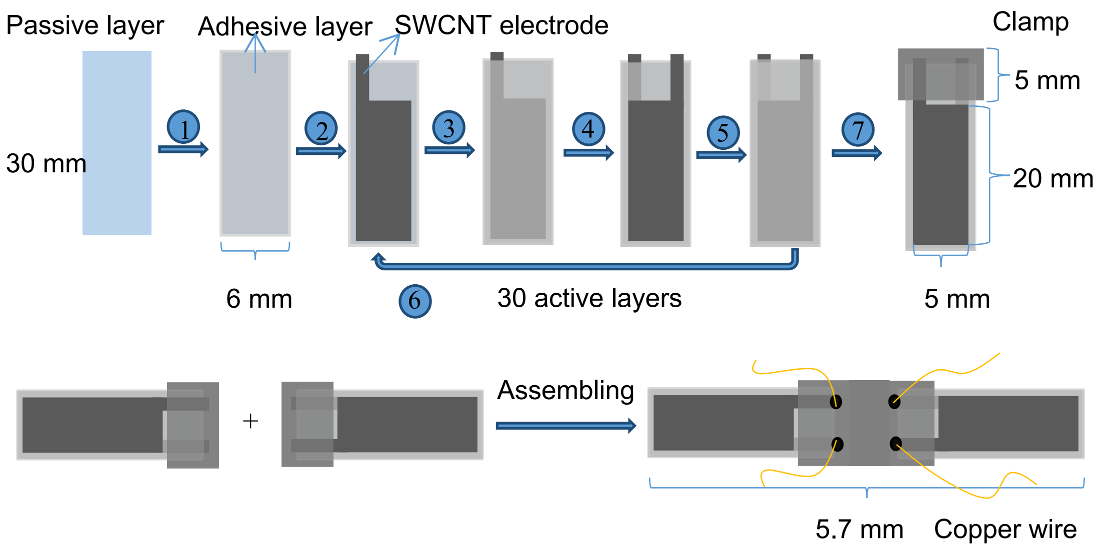

Fig. S22 The schematic illustration of preparing a directional soft robot.

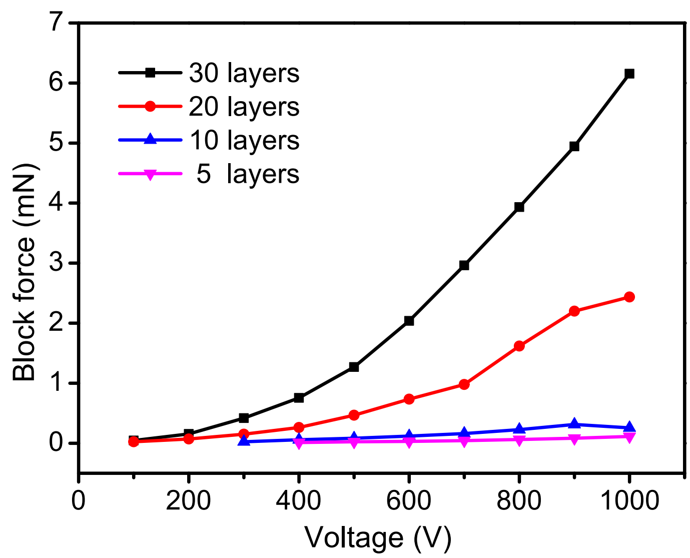

Fig. S23 The block force of bending actuators with different stacked layers was tested under different voltage.

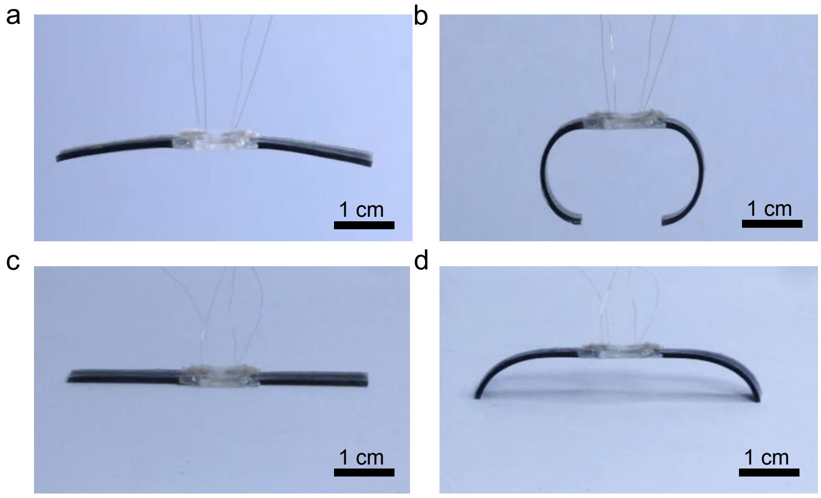

Fig. S24 A crawling robot assembled by two stacked bending actuators (30 active layers) was suspended in the air or laying on a paper under (**a**, **c**) static state and (**b**, **d**) actuated state (800 V), respectively.

Reference

[1] Z. Ma, Y. Xie, J. Mao, X. Yang, T. Li and Y. Luo, Macromol. Rapid Commun., 2017, 38, 1700268.

[2] S. Shian, R. M. Diebold, A. McNamara and D. R. Clarke, *Appl. Phys. Lett.,* 2012, 101, 061101.